J. Fluid Mech. (1986), *vol.* 163, *pp.* 323–347
Printed in Great Britain

Airfoils with separation and the resulting wakes

By TUNCER CEBECI,
Mechanical Engineering Department, California State University, Long Beach, California
R. W. CLARK, K. C. CHANG, N. D. HALSEY
Research and Technology, Douglas Aircraft Company, Long Beach, California
AND K. LEE
Mechanical Engineering Department, California State University, Long Beach, California

(Received 28 February 1985 and in revised form 1 August 1985)

A viscous/inviscid interaction method is described and has been used to calculate flows around four distinctly different airfoils as a function of angle of attack. It comprises an inviscid-flow method based on conformal mapping, a boundary-layer procedure based on the numerical solution of differential equations and an algebraic eddy viscosity. The results are in close agreement with experiment up to angles close to stall. In one case, where the airfoil thickness is large, small difficulties were experienced and are described. The method is shown to be capable of obtaining results with large flow separation and quantifies the role of transition on the lift coefficient.

1. Introduction

A natural procedure for calculating the pressure distribution on an airfoil requires the solution of inviscid- and viscous-flow equations. The viscous forces are first neglected and an inviscid pressure distribution determined. Boundary-layer equations are then solved from the stagnation point on both surfaces of the body and in the wake to provide distributions of displacement thickness which provide boundary conditions for a subsequent solution of inviscid-flow equations. This procedure is repeated until a converged solution of the pressure distribution is obtained. This iterative method provides a solution to the so-called 'weak-interaction' problem in which the flow remains largely attached. The more difficult 'strong-interaction' problem, in which there are significant regions of flow separation, is addressed in this paper.

For an iterative procedure to be successful, the displacement thickness must be determined accurately, and this involves the solution of laminar boundary-layer equations, the specification of transition, and the solution of equations appropriate to turbulent boundary layers and possibly to separated flows. While the calculation of laminar boundary layers depends mainly on the accuracy of numerical methods, the turbulent flows on the airfoil and in the wake require an accurate numerical method and appropriate assumptions for the Reynolds stresses. Previous investigations have shown that our ability to calculate turbulent wall boundary layers and wakes is satisfactory only where strong pressure gradients and separation are absent; see, for example, Cebeci & Meier (1979), Patel & Scheuerer (1982), and Chang *et al.* (1984). It should also be noted that, although the high angles of attack found in practice can lead to thick boundary layers, and possible separation, on the upper

surface with thin and even transitional boundary layers on the lower surface, no attempt to calculate such flows has been reported.

In recent years, strong-interaction procedures have been developed as useful methods for both low-speed flows about airfoils with high-lift devices and for transonic flows in which the interaction between a shock wave and a boundary layer can strongly influence the lift characteristics. Reviews of recent works are available in an AGARD Symposium volume (1981) and Cebeci (1984).

So far, most of the studies of the strong-interaction problem have concentrated on the development of methods for analysing airfoils with separation bubbles. After Briley & McDonald (1975) showed that the interactive boundary-layer approach could be used to compute transitional separation bubbles on airfoils, various investigators developed methods for analysing airfoils under similar flow conditions, making use of different numerical procedures for solving the boundary-layer equations, different methods for computing transition and different ways of handling the viscous/inviscid interaction. For example, Kwon & Pletcher (1979), Cebeci & Schimke (1983), Cebeci & Clark (1984), and Davis & Carter (1984) solved boundary-layer equations in differential form, whereas integral equations were used by Gleyzes, Cousteix & Bonnet (1984). To calculate transition, Kwon & Pletcher (1979) used an expression based on Michel's (1951) method and the e^9 method (see Cebeci & Bradshaw 1977); Cebeci *et al.* (1984) used the same formula for attached flows, and an expression given by Crimi & Reeves (1976) for flows with separation; Gleyzes *et al.* (1984) used the stability theory and, in some ways, the principles of the e^9 method; and Davis & Carter (1984) used the so-called McDonald– Fish–Kreskovsky (McDonald & Fish 1973; McDonald & Kreskovsky 1974) model which is based upon the solution of the integral form of the turbulent-kinetic-energy equation. The coupling between the inviscid- and viscous-flow methods has also been achieved in different ways. For example, Davis & Carter (1984) used a semi-inverse technique first proposed by LeBalleur (1978) and Carter (1979), whereas Cebeci (1984) and his associates utilized the scheme advocated by Veldman (1981) and by Cebeci, Stewartson & Williams (1981), and Gleyzes *et al.* (1984) made use of an inverse method coupled with a local approximation to an inverse inviscid-flow method utilizing the wall-transpiration model

$$v_n = \frac{\mathrm{d}}{\mathrm{d}s}(u_e \delta^*). \tag{1}$$

The present study extends those of Cebeci & Schimke (1983) and Cebeci & Clark (1984) to calculate the flow around an airfoil at angles of attack ranging from small to those corresponding to stall. The inviscid-flow procedures are described in §2. The basic viscous-flow equations, transformed equations and solution procedure are described in §3, which also considers the method of interaction with the external flow for the wall boundary layers and wake. Results are presented and discussed in §4 for several airfoils and angles of attack up to and including a stall angle. Summary conclusions are identified in §5.

2. Inviscid-flow method

The inviscid-flow method which is used here is based on conformal-mapping and Fourier-analysis techniques. These techniques, described in more detail by Halsey (1979), have a proven record of accuracy, efficiency and generality that makes them well suited for the current application.

The calculations can be divided conveniently into two nearly independent parts:

the transformation of the region outside the airfoil to the region outside the unit circle, and the determination of the flow solution in the transformed plane. The transformation is accomplished using a sequence of three conformal mappings. In the first mapping, the airfoil shape is perturbed slightly to make the upper- and lower-surface trailing-edge points coincide. This is accomplished using a logarithmic mapping function and is necessary only in those cases in which the airfoil trailing edge has non-zero thickness. In the second mapping, the trailing-edge corner is analytically removed by applying the Kármán–Trefftz mapping. In the final mapping, the resulting quasi-circular shape is mapped to a perfect circle using an iterated sequence of applications of the fast-Fourier-transform algorithm.

The calculation of the flow in the transformed plane also makes use of Fourier-analysis techniques. The complex velocity is expanded to give an infinite series involving a constant and negative powers of the complex coordinate. A finite number of the series coefficients are determined from the specified values of the normal velocity component at equally spaced points around the unit circle and from a Kutta condition which ensures stagnation at the trailing-edge point. The appropriate values for the normal-velocity-component boundary conditions are determined from previous viscous-flow calculations, using (1). For the initial inviscid-flow calculation in the interaction procedure, the specified normal velocity components may be taken from a previous calculation or they may simply be set to zero. In the latter case, a Fourier-analysis solution is not required and the classical analytic solution for flow over a circle is used.

For cases in which viscous wake effects are included, the flow-calculation procedure is slightly more complex. In these cases, the influence on the inviscid flow is simulated using a source/sink distribution along the inviscid trailing streamline and its reflection in the unit circle, which is required for the airfoil boundary condition. The local source density is determined using (1). The distribution is broken into piecewise linear segments and the flow due to the isolated-source distribution is computed using standard panel-method techniques. The total-flow solution in the transformed plane is then computed in the manner described above.

The major computational effort required in the inviscid-flow method is due to the transformations. In the viscous-/inviscid-flow interactions, it is necessary to compute the transformations only once, so that only the much faster flow calculations need to be repeated at each iteration. As a result, the computational expense due to the inviscid-flow calculations can be held to a minimum.

For flow at higher angles of attack care must be taken, since the displacement thickness at the trailing edge can become fairly large, approaching 10 % of the airfoil chord. The use of a blowing velocity on the airfoil surface produces a dividing streamline from the leading-edge stagnation point which approximates the edge of the boundary-layer displacement thickness. The inviscid flow outside this dividing streamline is therefore the same as that past the solid body defined by this streamline. However, inside this dividing streamline the inviscid flow is fictitious. In particular, near the trailing edge, the assumption that there is no pressure variation across this fictitious region becomes invalid as the magnitude of the blowing velocity v_n increases. The approach adopted here is, therefore, to evaluate the velocity distribution directly on the displacement surface while still applying the blowing velocity on the original airfoil surface. This is accomplished by mapping the displacement surface into the circle plane so that the Fourier series for the velocity can be evaluated directly on the displacement surface. If the Kutta condition is applied at the airfoil trailing edge then, in general, there will be a velocity discontinuity between the upper-

and lower-trailing-edge pressures. Therefore, the Kutta condition is modified to apply at the edge of the displacement surface using the same points as those at which the velocity is evaluated. The condition which is applied is that the off-body pressures computed at the upper- and lower-trailing-edge points are equal. This is accomplished by first computing the velocities at those off-body points with the total circulation specified by the previous inviscid calculation. A quadratic equation is then solved to compute the circulation required to make these two velocities equal. The effects of this Kutta condition will be discussed further in §4.1.

3. Interactive viscous-flow method

3.1. *Basic equations*

For two-dimensional external steady incompressible flows, the boundary-layer equations are well known and, with the concept of eddy viscosity ν_t and with b denoting $1+\nu_t/\nu$, can be written as

$$\frac{\partial u}{\partial x}+\frac{\partial v}{\partial y}=0, \tag{2}$$

$$u\frac{\partial u}{\partial x}+v\frac{\partial u}{\partial y}=u_e\frac{\mathrm{d}u_e}{\mathrm{d}x}+\nu\frac{\partial}{\partial y}\left(b\frac{\partial u}{\partial y}\right). \tag{3}$$

The boundary conditions for flow over an airfoil in the absence of mass transfer are

$$u=v=0, \quad \text{at } y=0, \tag{4a}$$

$$u\to u_e(x) \quad \text{as } y\to\infty. \tag{4b}$$

The boundary conditions for the wake require the specification of a dividing line, $y=0$, to separate the upper and lower parts of the inviscid flow. The normal pressure gradient across the shear layer is neglected and the boundary conditions become

$$u\to u_e(x) \quad \text{as } y\to\infty, \tag{5a}$$

$$v=0, \quad \text{at } y=0, \tag{5b}$$

$$u\to u_e(x) \quad \text{as } y\to-\infty. \tag{5c}$$

In these equations the external-velocity distribution $u_e(x)$ is obtained either from experiment or from inviscid-flow theory. In the latter case, it is often necessary to consider the effect of the displacement thickness on the calculated velocity distribution, and this can be done in several ways. Here, as in earlier references, we write the edge boundary condition, with $u_e^0(x)$ denoting the inviscid velocity distribution and $\delta u_e(x)$ the perturbation velocity due to viscous effects, as

$$u_e(x)=u_e^0(x)+\delta u_e(x), \tag{6}$$

and assume that the interaction region is limited to a finite range $x_a\leqslant x\leqslant x_b$. The perturbation velocity $\delta u_e(x)$ is determined from the Hilbert integral

$$\delta u_e(x)=\frac{1}{\pi}\int_{x_a}^{x_b}\frac{\mathrm{d}}{\mathrm{d}\sigma}(u_e\,\delta^*)\frac{\mathrm{d}\sigma}{x-\sigma}, \tag{7}$$

where $\mathrm{d}(u_e\,\delta^*)/\mathrm{d}\sigma$ is the blowing velocity. Following Cebeci & Clark (1984), we write (6) and (7) as

$$u_e(x)=u_e^0(x)+\sum_{j=1}^{n}c_{ij}(u_e\,\delta^*)_j. \tag{8a}$$

Here c_{ij} denotes the interaction-coefficient matrix, which is obtained from a discrete approximation to the Hilbert integral in (7). In this form, (8*a*) provides an outer boundary condition for the viscous-flow calculation which represents the viscous/inviscid interaction. It can be generalized to the form

$$u_e(x) = u_e^{\kappa}(x) + \sum_{j=1}^{n} c_{ij}[(u_e\,\delta^*)_j - (u_e\,\delta^*)_j^{\kappa}], \tag{8b}$$

where $u_e^{\kappa}(x)$ corresponds to the inviscid velocity distribution which contains the displacement-thickness effect $(\delta^*)^{\kappa}$ computed from a previous sweep, as we shall discuss later.

The presence of ν_t in *b* requires a turbulence model, and the algebraic eddy-viscosity formulation of Cebeci & Smith (1974) is used here. According to this formulation for wall boundary-layer flows, ν_t is defined by two separate formulas, given by

$$\nu_t = \begin{cases} \left\{0.4y\left[1-\exp\left(\dfrac{-y}{A}\right)\right]\right\}^2 \left|\dfrac{\partial u}{\partial y}\right| \gamma_{tr} \quad (0 \leqslant y \leqslant y_c), & (9a) \\ \alpha \left| \displaystyle\int_0^{\infty} (u_e - u)\,dy \right| \gamma_{tr}\,\gamma \quad (y_c \leqslant y \leqslant \delta), & (9b) \end{cases}$$

where

$$\left.\begin{aligned} A &= 26\nu u_\tau^{-1}, \quad u_\tau = \left(\frac{\tau_1}{\rho}\right)_{\max}^{\frac{1}{2}}, \\ \tau_1 &= \mu\frac{\partial u}{\partial y}, \quad \gamma = \frac{1}{1+5.5(y/\delta)^6}. \end{aligned}\right\} \tag{10}$$

The condition used to define y_c is the continuity of the eddy viscosity; from the wall outward (9*a*) is applied until its value is equal to the one given by (9*b*).

In (9), γ_{tr} is an intermittency factor which accounts for the transitional region that exists between a laminar and turbulent flow. It is given by

$$\gamma_{tr} = 1 - \exp\left[-G(x-x_{tr})\int_{x_{tr}}^{x} \frac{dx}{u_e}\right]. \tag{11a}$$

Here x_{tr} is the location of the start of transition and the empirical factor G is

$$G = \frac{1}{1200}\frac{u_e^3}{\nu^2} R_{x_{tr}}^{-1.34}, \tag{11b}$$

where the transition Reynolds number $R_{x_{tr}} = (u_e x/\nu)_{tr}$.

According to the Cebeci–Smith model, for values of R_θ greater than 5000, the parameter α in (9*b*) is equal to 0.0168 and, for R_θ less than 5000, it is given by the expression in Cebeci & Smith (1974). Studies conducted by Head (1976) and Nituch, Sjolander & Head (1978) and the recent experimental data of Nakayama (1982) and Simpson, Chew & Shivaprasad (1981) and the numerical studies of Carter (1981) indicate that, in flows with strong pressure gradient, the value of α should also be changed when $R_\theta > 5000$. Head and his associates recommend that α in (9*b*) be given by

$$\alpha = \alpha_{eq}\,F(r), \tag{12a}$$

where

$$\alpha_{eq} = 0.002094 + 0.02672[1-\exp(-0.1163G)], \tag{12b}$$

$$G = 4.8285\,(\Pi + 1.0717)^{\frac{1}{2}} + 1.8438, \tag{12c}$$

$$\Pi = \frac{\delta^*}{\tau_w}\frac{dp}{dx}, \tag{12d}$$

$$F = \begin{cases} \dfrac{(5-4r)}{(3-2r)} & (r < 1), \qquad (12e) \\ \dfrac{1}{2r-1} & (r \geqslant 1). \qquad (12f) \end{cases}$$

In (12e) and (12f), r represents the ratio of the local rate of growth of the boundary layer to the rate of growth of the corresponding equilibrium layer.

They also suggested that the intermittency term γ in (10) be replaced by

$$\gamma = \frac{2.0}{1-\mathrm{erf}[\frac{1}{2}(y/\delta-\beta)]}, \qquad (12g)$$

where β is a function of shape factor H.

Simpson *et al.* (1981) suggest that

$$\alpha = 0.0168/F^{2.5}. \qquad (13a)$$

Here F denotes the ratio of the product of the turbulent energy by normal stresses to that by shear stress evaluated at the location where shear stress is maximum, that is

$$F = \left\{\frac{(\overline{u'^2}-\overline{v'^2})\,\partial u/\partial x}{-\overline{u'v'}\,\partial u/\partial y}\right\}_{(-\overline{u'v'})_{\max}}. \qquad (13b)$$

Before (13a) can be used in (9b), an additional relationship between $(\overline{u'^2}-\overline{v'^2})$ and $(-\overline{u'v'})$ at $(-\overline{u'v'})_{\max}$ is needed. Here we assume that the ratio in (13b),

$$\beta = \left\{\frac{\overline{u'^2}-\overline{v'^2}}{-\overline{u'v'}}\right\}_{(-\overline{u'v'})_{\max}}, \qquad (13c)$$

is a function of $R_T = \tau_w/(-\overline{u'v'})_{\max}$ which, according to the data of Nakayama (1982), can be represented by

$$\beta = \frac{6}{1+2R_T(2-R_T)} \qquad (13d)$$

for $R_T < 1.0$, as shown in figure 1. For $R_T \geqslant 1.0$, we take β to be

$$\beta = \frac{2R_T}{1+R_T}. \qquad (13e)$$

Introducing the above relationships into the definition of F, we have the following expression for α, according to (13a),

$$\alpha = \frac{0.0168}{[1-\beta(\partial u/\partial x)/(\partial u/\partial y)]^{2.5}}, \qquad (14)$$

where β is given by (13d) and (13e). This expression is used here although further studies are clearly required to evaluate its range of validity. Work on this is in progress.

The eddy-viscosity formulation given by (9) should be modified for the wake calculation. The wake can be separated into two regions, the first of which is close to the trailing edge in which the flow is adjusting to the sudden elimination of the wall boundary condition at the trailing edge. Further downstream, in the far-wake region, Townsend (1956), after examining some early measurements in the wake of cylinders, suggested that

$$\nu_t = 0.032 u_e \theta, \qquad (15)$$

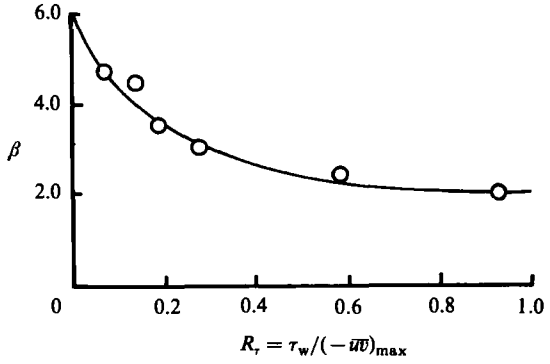

FIGURE 1. Relation between β and R_T according to the experimental data of Nakayama.

where θ is the momentum thickness

$$\theta = \int_{-\infty}^{\infty} \frac{u}{u_e}\left(1-\frac{u}{u_e}\right)\mathrm{d}y. \tag{16}$$

Equation (15) was later confirmed by Rodi (1975) from a survey of several sets of data and by Narasimha & Prabhu (1972) in more recent experiments. In the near wake, on the other hand, one would expect that the eddy viscosity should be close to that for the wall boundary layers near the trailing edge, while asymptotically approaching the far-wake expression downstream. Following the study reported by Chang *et al.* (1984), we have used the expression

$$\nu_t = \nu_w + (\nu_{te} - \nu_w)\,\mathrm{e}^{-B_1}, \tag{17}$$

where ν_{te} is the eddy viscosity at the trailing edge calculated from (9),

$$B_1 = (x - x_{te})/20\delta_{te},$$

and ν_w is the eddy viscosity for the far wake given by the maximum of ν_{wl} and ν_{wu} defined by

$$\left.\begin{aligned} \nu_{wl} &= 0.064 \int_{-\infty}^{y_{min}} (u_e - u)\,\mathrm{d}y, \\ \nu_{wu} &= 0.064 \int_{y_{min}}^{\infty} (u_e - u)\,\mathrm{d}y. \end{aligned}\right\} \tag{18}$$

Here the subscript l denotes the lower wake and u the upper wake. The location of y_{min} corresponds to $u = u_{min}$. It should be noted that expression (18) for the far wake is different from that suggested by Townsend (1956) so that it can apply to asymmetric wakes in which the velocities at the upper and lower edges could be different. In addition, the displacement thickness was used as the lengthscale instead of the momentum thickness because it was found by Chang *et al.* (1984) that it gave better results for wakes subject to adverse pressure gradients.

3.2. *Transformed equations*

Equations (2) and (3) may be solved in the forms presented in the previous section or they may be expressed in other forms which are more convenient and accurate for solution. Here, as in Cebeci & Schimke (1983), in the early stages of the flow, we use the Falkner–Skan transformation

$$\eta = \left(\frac{u_e}{\nu x}\right)^{\frac{1}{2}} y, \quad \psi = (u_e \nu x)^{\frac{1}{2}} f(x, \eta). \tag{19}$$

With primes denoting differentiation with respect to η, (2) and (3) and their boundary conditions on the airfoil can be written in the following form:

$$(bf'')' + \tfrac{1}{2}(m+1)ff'' + m[1-(f')^2] = x\left(f'\frac{\partial f'}{\partial x} - f''\frac{\partial f}{\partial x}\right), \tag{20}$$

$$\eta = 0, \quad f = f' = 0, \tag{21a}$$

$$\eta = \eta_e, \quad f' = 1. \tag{21b}$$

Here ψ is the usual definition of the stream function that satisfies the continuity equation

$$u = \frac{\partial \psi}{\partial y}, \quad v = -\frac{\partial \psi}{\partial x}, \tag{22}$$

and m is a dimensionless pressure-gradient parameter,

$$m = \frac{x}{u_e}\frac{\mathrm{d}u_e}{\mathrm{d}x}. \tag{23}$$

This transformation provides the generation of initial conditions at the stagnation point of the airfoil and allows the calculations to be performed economically and accurately around the leading edge, where the governing equations are being solved for the prescribed external-velocity distribution. For interactive boundary-layer calculations, where $u_e(x)$ is not known, a constant reference velocity u_0 is used in the transformation

$$Y = \left(\frac{u_0}{\nu x}\right)^{\frac{1}{2}} y, \quad \psi = (u_0 \nu x)^{\frac{1}{2}} F(x, Y). \tag{24}$$

In terms of these new variables, (2) and (3) and their boundary conditions can be written in the form:

$$(bF'')' + \tfrac{1}{2}FF'' + xw\frac{\mathrm{d}w}{\mathrm{d}x} = x\left(F'\frac{\partial F'}{\partial x} - F''\frac{\partial F}{\partial x}\right). \tag{25}$$

On the airfoil

$$Y = 0, \quad F = F' = 0, \tag{26a}$$

$$Y = Y_e, \quad F' = w, \quad w - \tilde{c}_{ii}(Y_e w - F) = g_i. \tag{26b}$$

In the wake

$$Y = -Y_e, \quad F' = w, \tag{27a}$$

$$\left.\begin{aligned} Y = 0, \quad F = 0, \\ Y = Y_e, \quad F' = w, \end{aligned}\right\} \tag{27b}$$

$$w - \tilde{c}_{ii}[w(Y_e - Y_{-e}) - (F_e - F_{-e})] = g_i, \tag{27c}$$

where

$$\tilde{c}_{ii} = c_{ii}\left(\frac{\nu x}{u_0}\right)^{\frac{1}{2}}.$$

Here w denotes the dimensionless external velocity u_e/u_0 and the parameter g_i, which results from the discrete approximation to the Hilbert integral (7), is given by

$$g_i = \overline{u}_e^{\kappa} + \sum_{j=1}^{i-1} c_{ij}(D_j - D_j^{\kappa}) - c_{ii} D_i^{\kappa}, \tag{28}$$

where

$$D = \left(\frac{\nu x}{u_0}\right)^{\frac{1}{2}} (Y_e w - F_e). \tag{29}$$

The expression for g_i on the wake is nearly identical to that for the airfoil, (28), except that now (29) is given by

$$D = \left(\frac{\nu x}{u_0}\right)^{\frac{1}{2}} [w(Y_e - Y_{-e}) - (F_e - F_{-e})]. \tag{30}$$

In the calculation of g_i on the wake an additional simplification is introduced in which the interaction region $[x_a, x_b]$ used in (7) is confined to the wake region itself. The effects of the airfoil boundary layer on the wake are fully accounted for after each complete sweep when the external velocity distribution is recomputed.

3.3. *Solution procedure*

The numerical solution of the system of equations given in the previous section for both the standard and interactive methods is obtained with Keller's box method. This is an efficient, second-order finite-difference method extensively used by Cebeci and his associates for a wide range of flows, as discussed in Bradshaw, Cebeci & Whitelaw (1981). The description of the standard method is given in that reference as well as in Cebeci & Bradshaw (1977). The general features of the inverse method, which makes use of the Mechul-function formulation, are also described for wall boundary layers in Bradshaw *et al.* (1981). As in previous studies the FLARE approximation is employed in which the convective term $\partial F'/\partial x$ is set equal to zero in the recirculating region, and no attempt was made to improve the accuracy of the solutions resulting from this approximation.

The solution procedure for the wake flow is novel and is described in the following paragraph. In general, airfoil wakes are considerably more difficult to calculate than wall boundary-layer flows, since at higher angles of attack they are strongly asymmetric and may involve the mixing of a thick separating turbulent boundary layer with a thin, possibly laminar, boundary layer. The change of boundary conditions from no slip on the body to smooth flow on the wake dividing streamline can cause numerical difficulties. We observe from (27*c*) that the solution of (25) for two wake-edge quantities, F_e and F_{-e}, both of which can be large, may affect the rate of convergence of the solution. In addition, the calculation of wakes with various degrees of flow separation and the use of the FLARE approximation for such flows has not previously been explored.

As in the solution of wall boundary-layer flows by Keller's method, we write (25) as a first-order system. For this purpose we let

$$F' = u, \tag{31a}$$

$$u' = v, \tag{31b}$$

and write (25) as

$$(bv)' + \tfrac{1}{2}Fv + xw\frac{\mathrm{d}w}{\mathrm{d}x} = x\left(u\frac{\partial u}{\partial x} - v\frac{\partial F}{\partial x}\right). \tag{31c}$$

In order to obtain stable solutions to the above equations and to reduce their sensitivity to the boundary conditions which involve F_e and F_{-e}, we make use of the Mechul-function formulation and denote F_{-e} by s. Since both s and w are functions of x only, we write

$$s' = 0 \tag{31d}$$

and

$$w' = 0. \tag{31e}$$

The boundary conditions for the system given by (31) now can be written as

$$Y = Y_{-e}, \quad u = w, \quad s = F_{-e}, \tag{32a}$$

$$Y = 0, \quad F = 0, \tag{32b}$$

$$\left.\begin{aligned} Y = Y_e, \quad & u = w, \\ & w - \tilde{c}_{it}[w(Y_e - Y_{-e}) - (F - s)] = g_i. \end{aligned}\right\} \tag{32c}$$

The system of (28) and (29) can now be solved by the procedure described in Bradshaw *et al.* (1981). After the finite-difference approximations to (31) and (32) are written, the resulting nonlinear algebraic system is linearized by Newton's method and the linear system is then solved by the block-elimination method.

4. Results and discussion

The first step in the solution procedure requires the calculation of the inviscid-flow equations for the known airfoil shape, angle of attack and free-stream velocity. With the resulting pressure distribution, the laminar-boundary-layer equations are solved from the leading edge along both surfaces for a short distance. The standard boundary-layer approach is replaced by the inverse approach and is used to calculate laminar as well as turbulent flows with separation, with transition location either specified or computed by an empirical formula. The calculations include both wall-boundary-layer and wake flows. In general, at lower angles of attack we use approximately 60 x-stations, each on the upper and lower surfaces of the airfoil, and 30 in the wake. At higher angles of attack, the number of x-stations on the upper surface is increased to around 80, while the number of stations on the lower surface and wake remains unchanged. The point distribution on the airfoil is chosen such that the distribution is fine near the leading and trailing edges and somewhat coarse in between. The interaction coefficients on the airfoil are computed from the specified distributions of x-stations.

As the two wall boundary layers merge into a wake, the boundary conditions change suddenly from the no-slip conditions in which $u = 0$ at $y = 0$ to a finite velocity on the dividing streamline in the wake. In order to account for this 'jump', it is necessary to use very small step sizes immediately downstream of the trailing edge. Based on the mixing-length theory for the wall boundary layers, Burgraff (1974) obtained the centreline velocity $u_c(x)$ for turbulent flow downstream of a flat plate as

$$u_c(x) = 0.1542 R_0^{\frac{1}{8}} \xi + O(\xi^3). \tag{33}$$

Here $\xi = (x - x_0)^{\frac{1}{3}}$ with $x_0 = 1$ at the trailing edge and R_0 is the Reynolds number based on the plate length. It is seen that a step size

$$\Delta x = R_0^{-\frac{3}{5}} \tag{34}$$

corrresponds to a 15% increase in the centreline velocity over the first step. For $R_0 = 10^6$, the corresponding Δx is around 0.00025. In all the wake calculations, we have used (34) as the criterion to determine the first step size.

There are several empirical methods for computing transition on airfoils, such as those based on Michel's correlation method (1974) and the e^9 method based on the linear stability theory. Both methods produce results which are satisfactory for most airfoil flows without separation, but Michel's method is not valid for flows with separation while the extension of the e^9 method for such flows has not been explored.

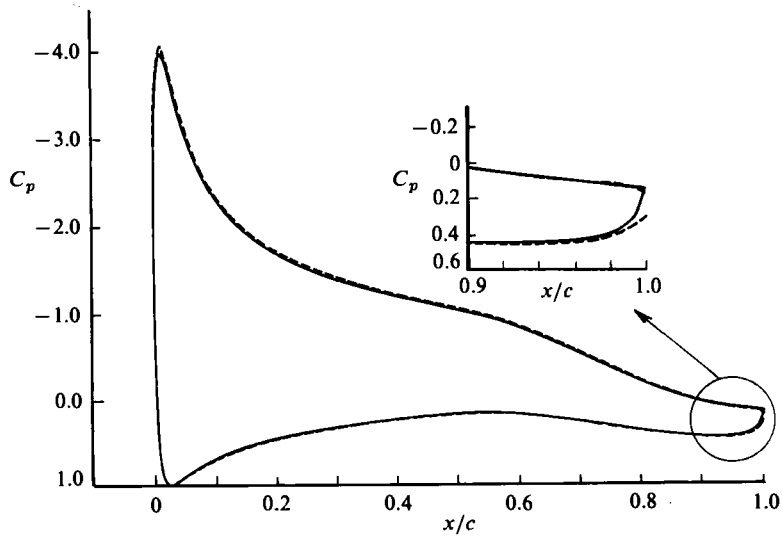

FIGURE 2. Comparison of on-body (– – –) and off-body (——) Kutta condition – GA(W)-1 airfoil, $\alpha = 10°$, $R_c = 5.7 \times 10^6$.

An empirical method has been proposed by Crimi & Reeves (1976) to represent transition in a separation bubble, but it has not been verified for flows with large separation. A common procedure in calculating transition in flows with separation, especially flows at higher angles of attack, is to assume that laminar separation is the transition location.

In the present paper we use Michel's method and compute transition from the following formula given in Cebeci & Bradshaw (1977):

$$R_\theta = 1.174\left(1+\frac{22400}{R_x}\right)R_x^{0.46}. \tag{35}$$

When flow separation takes place upstream of the transition location predicted by (35) then transition is assumed to occur. This choice, while satisfactory for high-Reynolds-number flows, is not a good one in general since the laminar separation point is independent of the Reynolds number, but for low-Reynolds-number flows, where experiments indicate large separation bubbles, the transition location is well within the bubble.

4.1. *Numerical features of the method*

In §2 it was stated that the calculation of the potential-flow solution required the use of an off-body velocity evaluation in which both the Kutta condition and the pressures are evaluated on the edge of the displacement thickness. Figures 2 and 3 provide a comparison between computed pressure distributions obtained using on-body and off-body evaluations. These results were obtained for the GA(W)-1 airfoil for $R_c = 5.7 \times 10^6$. Figure 2 shows the pressures for $\alpha = 10°$ for which the flow is separated over the last 5 % of the upper surface, and the trailing-edge displacement thickness is about 2 % of the airfoil chord. Under these conditions the effect of the off-body Kutta condition is relatively minor, the only noticeable differences occurring very close to the trailing edge. As the angle of attack increases, the effects become more significant. Figure 3 shows the computed pressures for $\alpha = 15°$ in which the separation region extends over the last 15 % of the airfoil, with a trailing-edge

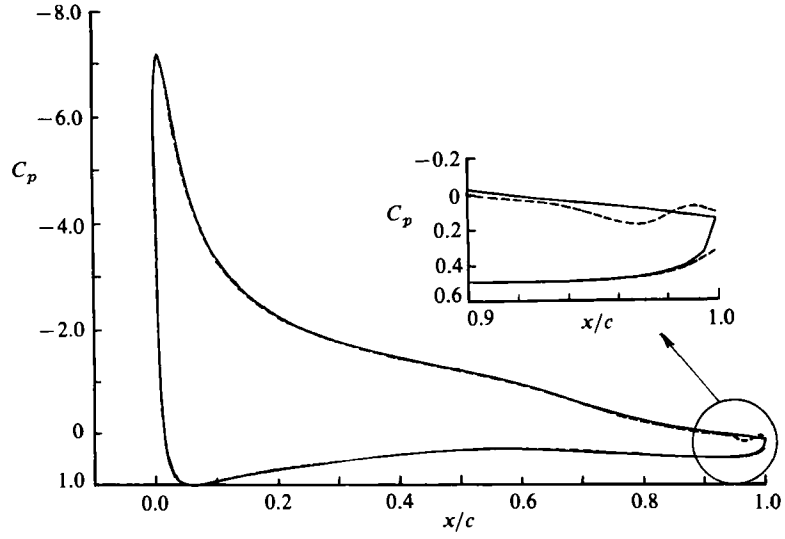

FIGURE 3. Comparison of on-body (– – –) and off-body (——) Kutta condition – GA(W)-1 airfoil, $\alpha = 15°$, $R_c = 5.7 \times 10^6$.

displacement thickness of about 3% chord. For this case, it can be seen that the velocities evaluated on the airfoil surface give some undesirable pressure gradients in the trailing-edge region, which are avoided through the evaluation of the velocities on the displacement surface.

In order to increase the rate of convergence of the viscous/inviscid cycles, an over-relaxation scheme has been incorporated. This scheme makes use of a relaxation formula similar to that which Carter (1979) used to update the mass flux. After each sweep the computed blowing velocity is updated using the formula

$$v_n^{\kappa+1}(x) = v_n^{\kappa}(x)\left[1+\omega\left(\frac{u_{e_v}}{u_{e_i}}-1\right)\right], \tag{36}$$

where $v_n^{\kappa}(x)$ is the blowing velocity computed from the current displacement thickness and $v_n^{\kappa+1}(x)$ is the modified distribution which is used to compute the new inviscid velocity. In this equation, u_{e_v} is the external velocity distribution computed by the inverse boundary-layer solution and u_{e_i} is the velocity computed by the previous potential-flow solution. Figures 4 and 5 illustrate the effect of the relaxation parameter ω on the rate of convergence of the solution for the flow over the NACA 0012 airfoil, for $\alpha = 10°$ and $R_c = 6.0 \times 10^6$. Figure 4 shows the computed c_l after each iteration without acceleration ($\omega = 0$), and with acceleration ($\omega = 2$). The corresponding upper-surface and wake-displacement-thickness distributions are shown in figure 5.

Another effective way of improving the rate of convergence is provided by including some approximation to the viscous effects in the original potential-flow solution rather than starting from a purely inviscid velocity distribution. This is accomplished here by taking an initial displacement thickness from a converged solution at a lower angle of attack. Figure 6 shows the computed c_l at $\alpha = 10°$ using an initial solution computed for $\alpha = 9°$. Comparison with figure 4 shows that the use of a non-zero starting solution significantly reduces the number of iterations required for convergence. Figure 7 shows the displacement thickness computed on the NACA

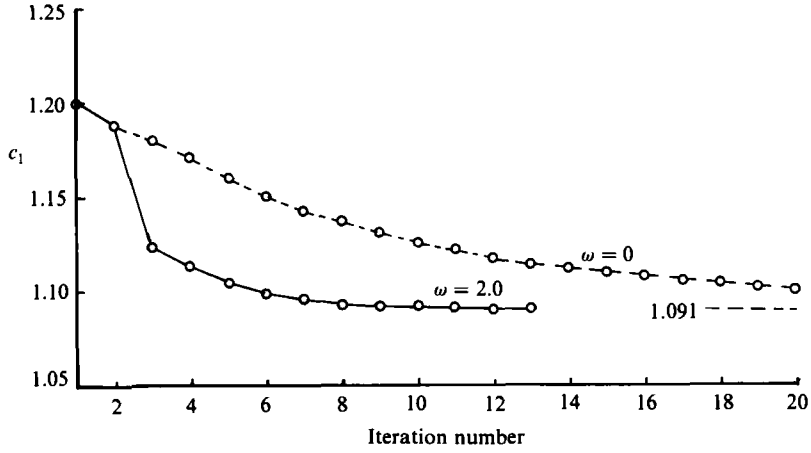

FIGURE 4. The variation of c_l with iteration number – NACA 0012 airfoil, $\alpha = 10°$, $R_c = 6.0 \times 10^6$.

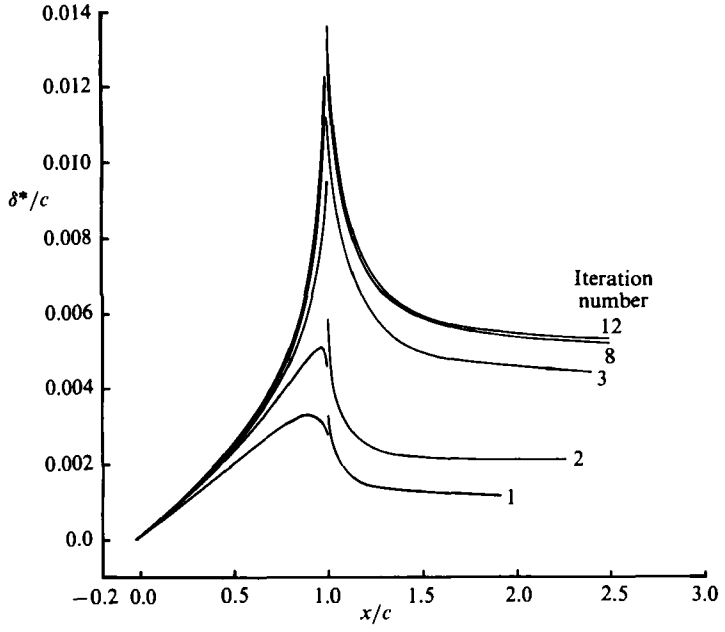

FIGURE 5. The distribution of displacement thickness along the upper surface and wake – NACA 0012 airfoil, $\alpha = 10°$, $R_c = 6.0 \times 10^6$.

0012 airfoil using this approach. In each case the converged solution required fewer than 10 iterations.

The relative importance of calculations in the wake at high angles of attack is demonstrated by figures 8 and 9. Figure 8 shows the computed separation location on the airfoil. When the wake is included, separation is encountered for angles of attack greater than 11°, and attempts to obtain results without consideration of the wake led to erroneously large regions of recirculation. Figure 9 shows that the difference in displacement thickness at the trailing edge is negligible for $\alpha = 10°$, but more than 30% for $\alpha = 16°$.

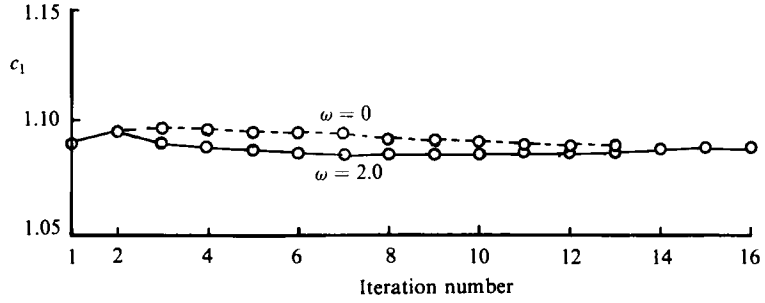

FIGURE 6. The variation of c_l with iteration number – NACA 0012 airfoil, $\alpha = 10°$, $R_c = 6.0 \times 10^6$. (Initial δ^* values from $\alpha = 9°$.)

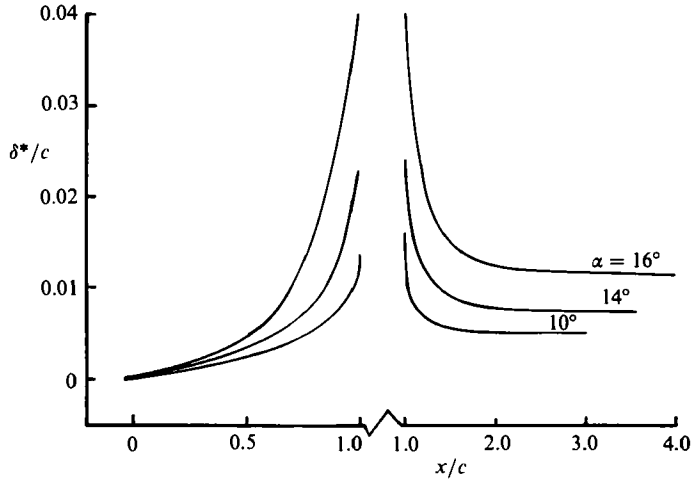

FIGURE 7. The displacement thickness distributions along the upper surfaces and wakes – NACA 0012 airfoil, $R_c = 6.0 \times 10^6$.

In order to perform the calculations in the presence of separation, the FLARE approximation was used and proved to be satisfactory when the separation region was small. As the extent of the separation region increased an additional iterative scheme, based on the homotopy continuation method, was introduced at the start of the wake calculation. Under this scheme an initial velocity profile at the trailing edge was defined by

$$u = u_{\text{ref}} + n(u - u_{\text{ref}}), \quad n = 0, 0.50, 1.0, \tag{37}$$

and the boundary-layer solution was computed at the first point on the wake with $\eta = 0$. Here u_{ref} corresponds to a non-separating velocity profile constructed somewhat arbitrarily from the separated velocity profile at the trailing edge. This solution was then repeated with $n = 0.50$ and 1.0 until the solutions converged. This procedure was applied for each velocity profile in the wake with separation. This procedure was necessary for angles of attack greater than 15°. Attempts to avoid the problem by approaching from lower angles of attack with smaller increments of angle were unsuccessful.

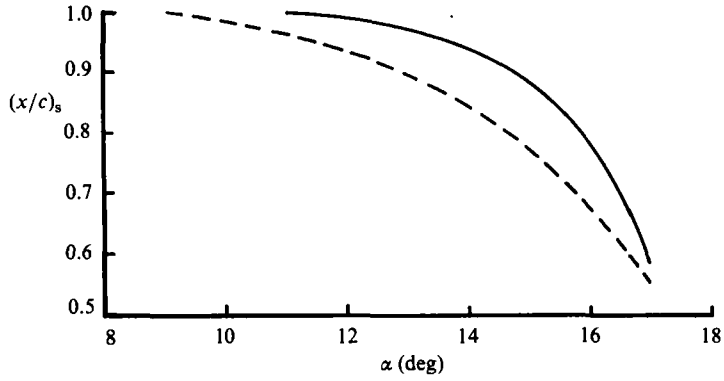

FIGURE 8. Effect of wake on the separation region – NACA 0012 airfoil, $R_c = 6.0 \times 10^6$. ——, with wake; - - - -, without wake.

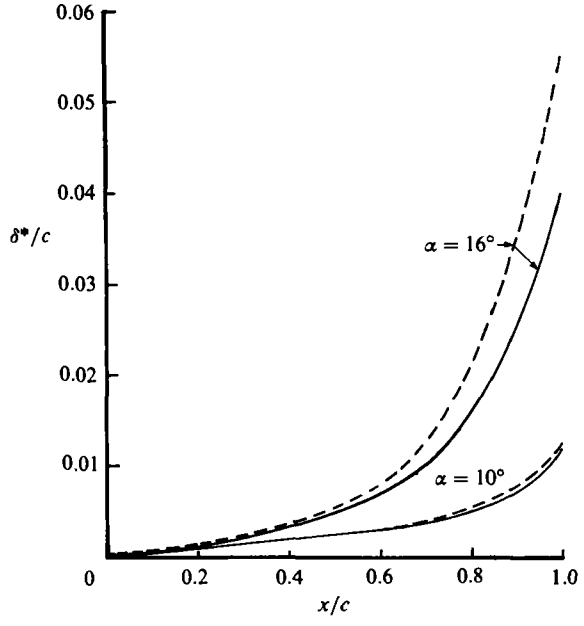

FIGURE 9. The effect of wake on displacement thickness – NACA 0012 airfoil, $R_c = 6.0 \times 10^6$. ——, with wake; - - - -, without wake.

4.2. *Comparison with experiment*

Calculations have been performed for several airfoils and are presented in the following paragraphs in a sequence which corresponds to the complexity of the flow. Thus the first results are presented for a symmetrical airfoil, NACA 0012, at angles of attack up to and including stall. The second airfoil, NACA 4412, has camber, and the measurements again correspond to angles of attack up to and including stall. Finally, results are presented for two aft-loaded airfoils, GA(W)-1 and GA(W)-2, which are 17 % and 13 % thick respectively. These airfoils have been investigated for angles of attack up to 16°. In all cases, the chord Reynolds numbers imply that transition can play an important role, and it was treated here in the manner described previously.

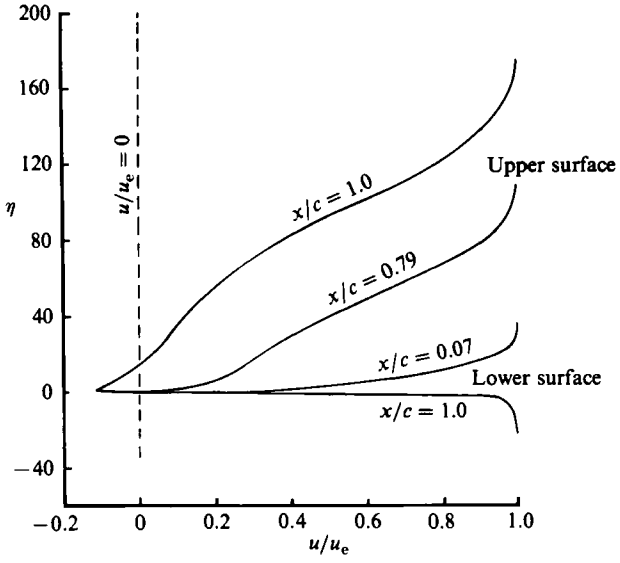

FIGURE 10. Velocity profiles along the upper and lower surfaces – NACA 0012 airfoil, $\alpha = 16°$, $R_c = 6.0 \times 10^6$.

Results for the NACA 0012 airfoil are shown in figures 10–13. Figures 10 and 11 show the computed velocity profiles on the airfoil and in the wake at $\alpha = 16°$. The computed lift and drag curves are compared with experimental measurements (Abbott & von Doenhoff 1959) in figures 12 and 13. As can be seen from figure 12, the calculated results are in very good agreement with measurements up to $\alpha = 15°$. The calculations suggest that stall occurs for α beyond 19°, whereas the experiments indicate stall for $\alpha > 16°$. As shown in the figure, a very small adjustment to the location of transition results in calculations of stall angle in accord with measurements. To further elaborate on this point and to show the role of transition, table 1 presents calculated results for three angles of attack. Those in table 1 (*a*) were obtained for $\alpha = 6°$ with the transition location computed from (35). As can be seen from the values of c_l and displacement thickness at the trailing edge, movement of the transition location by 2 % of chord has a negligible effect.

Location of transition at $x/c = 0.078$, however, leads to a breakdown in the solutions for reasons consistent with those found by Cebeci & Schimke (1983). In an adverse pressure gradient, as in this case, for the solutions to exist it appears that transition must occur upstream of some limiting location.

The same phenomenon is evident in table 1 (*b*), which corresponds to $\alpha = 12°$ and a much higher lift coefficient. In this case, transition was assigned to the location corresponding to laminar separation since (35) was inappropriate. A small adjustment to the location of transition has a small effect on lift. In these tables, negative values of x/c imply that the point is on the geometric lower surface of the airfoil. Movement of transition to $x/c = 0.0170$, as with $\alpha = 6°$, causes the solutions to break down. In contrast, the results for $\alpha = 17°$ shown on table 1 (*c*) indicate that the lift coefficient is strongly dependent on the location of transition. In this case the extent of the region of trailing-edge separation is large, and becomes larger as the transition location is moved upstream. Consistent with this result, the displacement thickness at the trailing edge increases and the lift coefficient decreases as the transition location moves upstream.

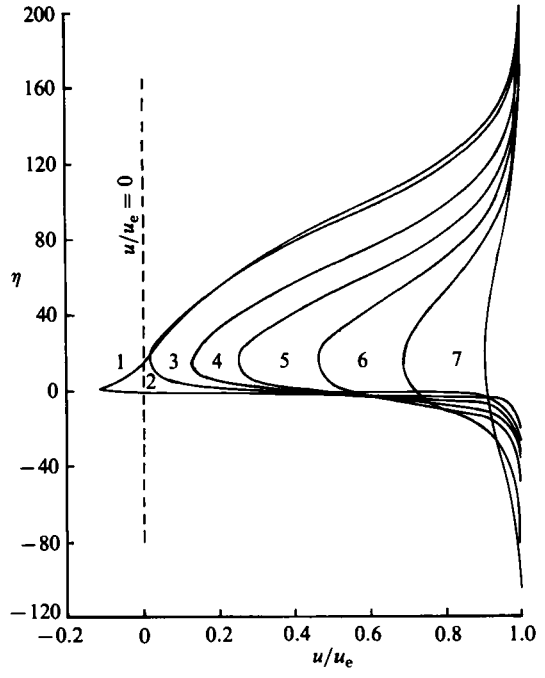

FIGURE 11. Velocity profiles on the wake region – NACA 0012 airfoil, $\alpha = 10°$, $R_c = 6.0 \times 10^6$. Curve 1, $x/c = 1.001$; 2, 1.029; 3, 1.079; 4, 1.122; 5, 1.226; 6, 1.500; 7, 4.248.

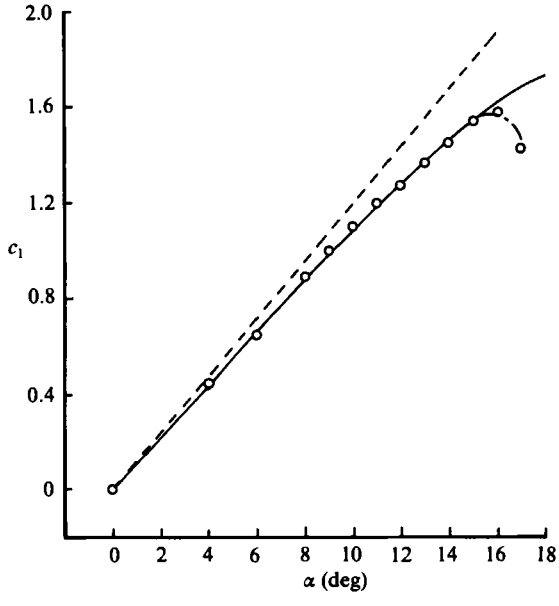

FIGURE 12. Variation of c_l with α – NACA 0012 airfoil, $R_c = 6.0 \times 10^6$. – – –, inviscid; ——, interactive theory; — — —, interactive theory (modified transition); ○, experimental data.

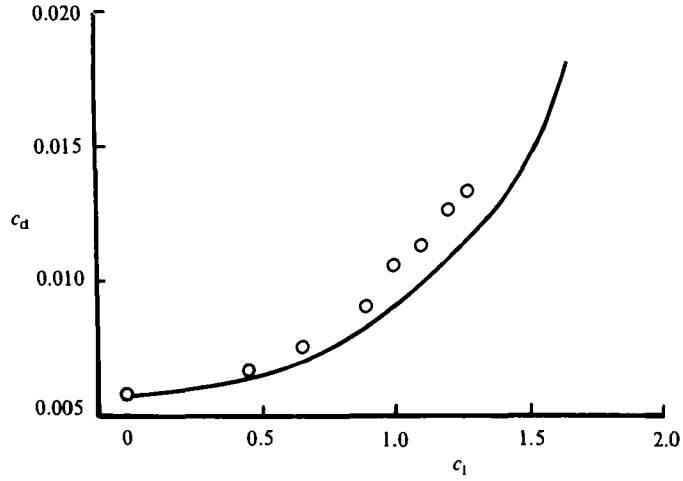

FIGURE 13. Variation of c_d with c_l – NACA 0012 airfoil, $R_c = 6.0 \times 10^6$. ——, interactive theory; ○, experimental data.

(*a*) $\alpha = 6°$. Experimental value of $c_l = 0.65$. Transition computed from (35).

$\left(\frac{x}{c}\right)_{tr}$	c_l	$\left(\frac{\delta^*}{c}\right)_{te}$
0.031 (fixed)	0.625	0.0091
0.052 (computed)	0.628	0.0089
0.070 (fixed)	0.633	0.0084
0.078 (fixed)	—	—

(*b*) $\alpha = 12°$. Experimental value of $c_l = 1.29$. Transition location corresponds to laminar separation.

$\left(\frac{x}{c}\right)_{tr}$	c_l	$\left(\frac{\delta^*}{c}\right)_{te}$	$\left(\frac{\Delta x}{c}\right)_{sep}$
−0.0030 (fixed)	1.270	0.0195	0.965 ~ TE
0.0025 (fixed)	1.283	0.0172	0.986 ~ TE
0.0083 (computed)	1.286	0.0167	0.986 ~ TE
0.0170 (fixed)	—	—	—

(*c*) $\alpha = 17°$. Experimental value of $c_l = 1.42$. Computed transition location corresponds to laminar separation.

$\left(\frac{x}{c}\right)_{tr}$	c_l	$\left(\frac{\delta^*}{c}\right)_{te}$	$\left(\frac{\Delta x}{c}\right)_{sep}$
−0.0173 (fixed)	1.502	0.0768	0.56 ~ TE
−0.00925 (fixed)	1.514	0.0737	0.60 ~ TE
−0.00250 (fixed)	1.573	0.0615	0.66 ~ TE
0.000493 (computed)	1.669	0.0453	0.77 ~ TE

TABLE 1. Effect of transition on the flow properties of an NACA 0012 airfoil for $R_c = 6 \times 10^6$

Figure 13 shows calculated and measured variations of total drag coefficient versus lift coefficient. The discrepancies increase with angle of attack and are undoubtedly due in part to measurement accuracy. In addition, the accuracy of the calculations in the wake region requires further examination of numerical uncertainties and of those due to the neglect of normal pressure gradient.

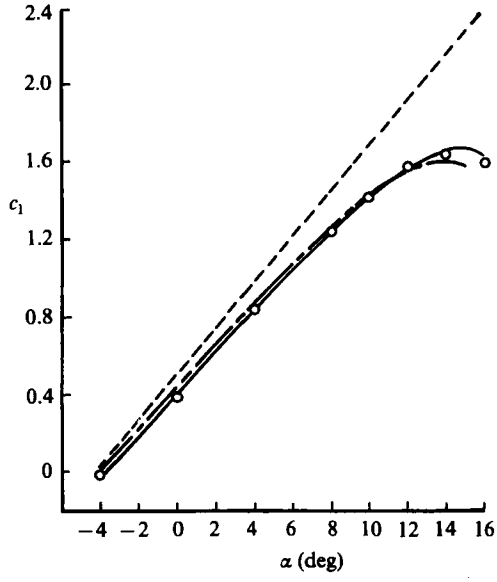

FIGURE 14. Variation of c_l with α – NACA 4412 airfoil, $R_c = 1.523 \times 10^6$. (Modified transition corresponds to experimental location.) – – –, inviscid; ——, interactive theory; — – —, interactive theory (modified transition; ○, experimental data.

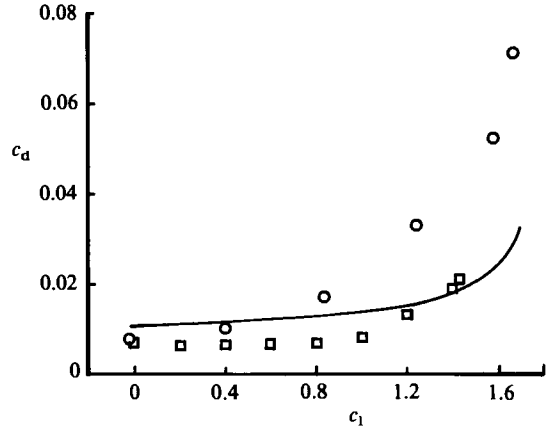

FIGURE 15. Variation of c_d with c_l – NACA 4412 airfoil, $R_c = 1.523 \times 10^6$. ——, interactive theory; ○, data of Wadcock (1978); □, data of Abbott & von Doenhoff (1959).

In the experiments of Wadcock (1978) and Coles & Wadcock (1979), a flying hot-wire arrangement was used to measure the velocity characteristics of the flow around an NACA 4412 airfoil at angles of attack up to that corresponding to maximum lift. The results in figures 14–16 show the experimental and computed lift and drag curves and the pressure distribution respectively. Figures 14 and 15 were obtained with transition locations corresponding both to the procedure described earlier and to that obtained by the tripping arrangement of the experiment. The measured and calculated values of c_l are in close agreement up to $\alpha = 12°$, with those corresponding to experimentally determined transition in slightly better agreement. The drag curves, shown in figure 15, agree fairly well at low values of c_l and poorly at higher

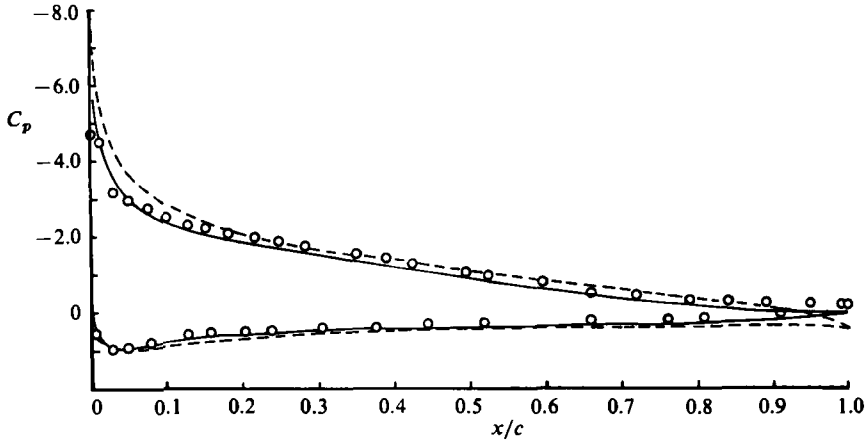

FIGURE 16. Variation of C_p with x/c – NACA 4412 airfoil, $\alpha = 12°$, $R_c = 1.523 \times 10^6$. – – –, inviscid; ——, interactive theory; ○, experimental data.

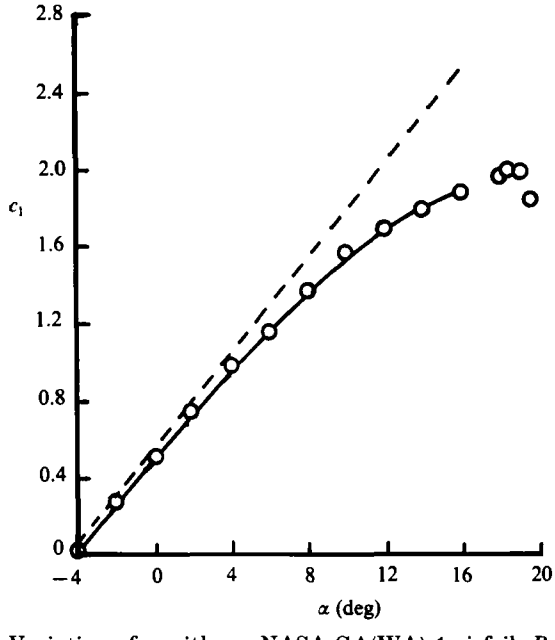

FIGURE 17. Variation of c_l with α – NASA GA(WA)-1 airfoil, $R_c = 5.7 \times 10^6$. – – –, inviscid; ——, interactive theory; ○, experimental data.

values. It should be noted, however, that two different sets of experimental data at slightly different Reynolds numbers differ significantly. The results in figure 16 confirm the close agreement between measurements and calculations of the distribution of pressure coefficient. It is clear that the inclusion of viscous effects influences the pressure distribution considerably in the leading- and trailing-edge regions.

The measurements of McGhee & Beasley (1973) were obtained for the flow around the 17% thick NASA GA(W)-1 airfoil as a function of angle of attack and Reynolds number. Results were obtained with natural transition and with 0.25 cm wide transition strips located at 0.08c. They are shown in figures 17 and 18 in terms of lift coefficient and drag coefficient and agree well with calculations up to $\alpha = 16°$.

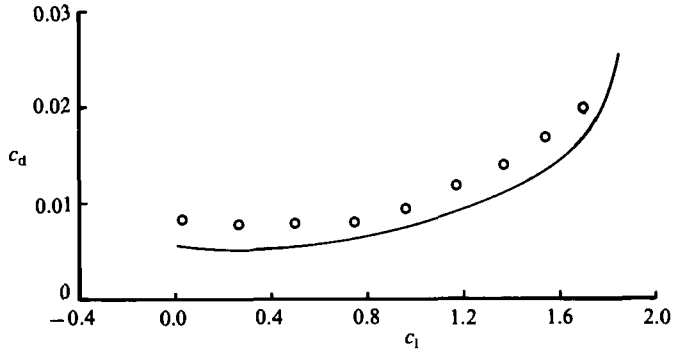

FIGURE 18. Variation of c_d with c_l – NASA GA(WA)-1 airfoil, $R_c = 5.7 \times 10^6$. ——, interactive theory; O, experimental data.

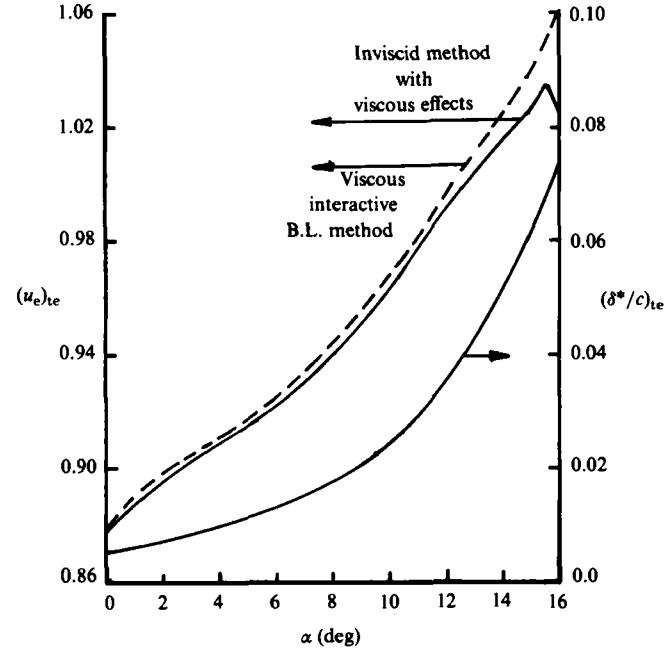

FIGURE 19. Comparison of inviscid and boundary-layer edge velocities at the trailing edge – GA(W)-1 airfoil, $R_c = 5.7 \times 10^6$.

Perhaps due to the thicker airfoil, and much increased displacement thickness at the trailing edge, some difficulties were experienced in performing the calculations beyond 13°, and no attempt was made to extend them to angles greater than 16°. The nature of the difficulties encountered is illustrated by figure 19, which plots the computed external velocity at the trailing edge against angle of attack. This figure shows the velocities computed by both the potential-flow and the boundary-layer solutions. As the solution converges, these two values should agree. The level of agreement seen here below $\alpha = 13°$ is very good and is consistent with that observed on the previous two airfoils at all angles of attack. For this airfoil, however, the agreement deteriorates at the larger angles.

Figures 20–22 compare results for the present method for the 13 % thick GA(W)-2

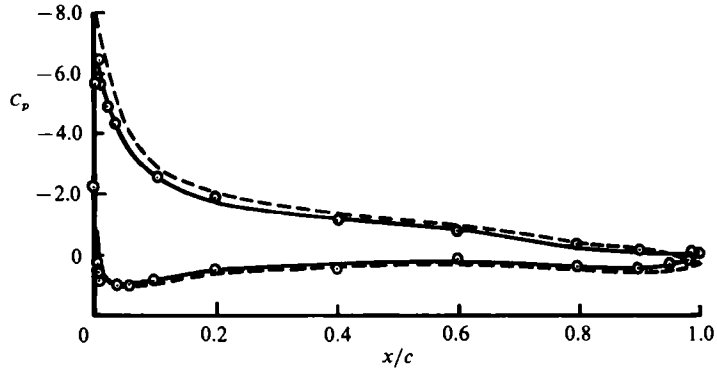

FIGURE 20. Variation of C_p with x/c – GA(W)-2 airfoil, $\alpha = 12°$, $R_c = 4.3 \times 10^6$. – – –, inviscid; ——, interactive theory; ○, experimental data.

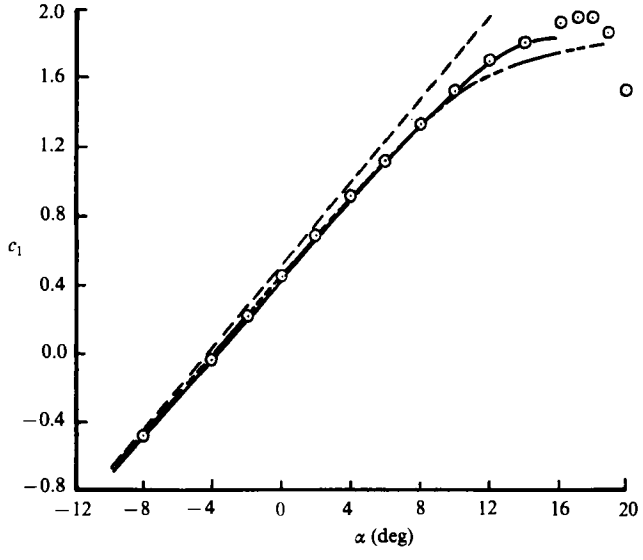

FIGURE 21. Variation of c_l with α – GA(W)-2 airfoil, $R_c = 4.3 \times 10^6$. – – –, inviscid; ——, interactive theory (present method); ———, interactive theory (Melnik & Brook 1986); ○, experimental data.

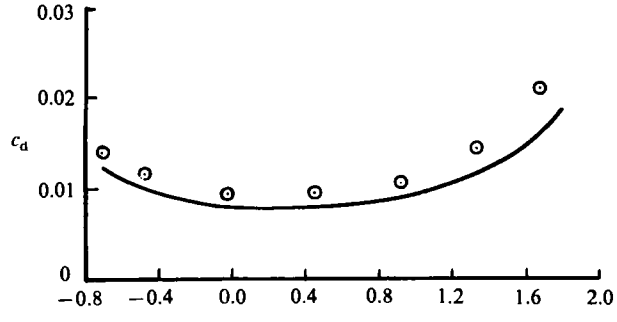

FIGURE 22. Variation of c_d with c_l – GA(W)-2 airfoil, $R_c = 4.3 \times 10^6$. ——, interactive theory; ○, experimental data.

airfoil with the experimental data of McGhee, Beasley & Somers (1977). The pressure distribution, shown in figure 20 for $\alpha = 12°$, agrees well with the experimental data, showing that the present interactive theory can give a good prediction of the viscous effect. The lift-curve slope is shown in figure 21, from which it can be seen that the present method gives good agreement up to about a 16° angle of attack. Results obtained by Melnik & Brook (1986) using the GRUMFOIL program agree well with the experimental data up to about 10°, after which there is some deviation, perhaps due to the nature of their boundary-layer method or their treatment of the wake. The variation of drag with lift, presented in figure 22, shows that the present method predicts the drag very well over the whole range considered.

5. Concluding remarks

The following more important conclusions can be extracted from the preceding sections.

(i) The iterative procedure has been demonstrated to allow calculations of the flow properties around four airfoils and over a wide range of angles of attack. Comparison with measurements shows excellent agreement up to angles close to stall.

(ii) The flows investigated involved large regions of trailing-edge separation, and calculations were extended into the wake with the assistance of a special numerical procedure.

(iii) The results show that the location of transition has an increasing influence on the flow properties as the angle of attack approaches stall. It has also been shown that calculations break down with assigned transition locations which appeared to be unrealistic.

(iv) Further work is required to evaluate the influence of normal pressure gradient and to resolve the difficulties which arose with the thickest airfoil at high angles of attack.

It has also been found that the present interactive scheme is well suited for transonic flows. Cebeci, Clark & Chang (1986) report results for two-dimensional transonic flows which indicate good agreement with experiment. An adaptation of this scheme in a strip-theory approximation produced equally good results for three-dimensional transonic flows as reported by Cebeci, Chen & Chang (1986).

In a related study reported by Mehta, Chang and Cebeci (1986), a comparison between the predictions of the present interacive procedure and the thin Navier–Stokes solutions was made for the NACA 0012 airfoil. It was found that, when the same turbulence model and transition assumptions were used, the predictions of both methods agreed well, demonstrating the validity of the use of interactive boundary-layer theory for flows with large regions of separation.

The research reported in this paper was sponsored by the National Science Foundation, under Grant MEA 0818565.

REFERENCES

ABBOTT, J. H. & VON DOENHOFF, A. E. 1959 *Theory of Wing Sections*. Dover.

AGARD 1981 Computation of viscous–inviscid interactions. *AGARD CP-291*.

BRADSHAW, P., CEBECI, T. & WHITELAW, J. H. 1981 *Engineering Calculation Methods for Turbulent Flows*. Academic.

BRILEY, W. E. & MCDONALD, H. 1975 Numerical prediction of incompressible separation bubbles. *J. Fluid Mech.* **69**, 631.

BURGRAFF, O. R. 1974 Comparative study of turbulent models for boundary layers and wakes. *Aero. Res. Lab.* 74-0031.

CARTER, J. E. 1979 A new boundary-layer inviscid iteration technique for separated flow. *AIAA Paper* 75-1450.

CARTER, J. E. 1981 Viscous–inviscid interaction analysis of transonic turbulent separated flow. *AIAA Paper* 81-1241.

CEBECI, T. 1976 Separated flows and their representation by boundary-layer equations. *Mech. Engng Dept Rep.* ONR-CR215-234–2, California State University, Long Beach.

CEBECI, T. (ed.) 1984 *Numerical and Physical Aspects of Aerodynamic Flows*, vol. II. Springer.

CEBECI, T. & BRADSHAW, P. 1977 *Momentum Transfer in Boundary Layers.* Hemisphere.

CEBECI, T., CHEN, L. T. & CHANG, K. C. 1986 An interactive scheme for three-dimensional transonic flows. In *Numerical and Physical Aspects of Aerodynamic Flows*, vol. III (ed. T. Cebeci), Springer.

CEBECI, T. & CLARK, R. W. 1984 An interactive approach to subsonic flows with separation. In *Numerical and Physical Aspects of Aerodynamic Flows*, vol. II (ed. T. Cebeci), p. 194. Springer.

CEBECI, T., CLARK, R. W. & CHANG, K. C. 1986 On the solution of transonic flows with viscous effects (to be published).

CEBECI, T. & MEIER, H. U. 1979 Modelling requirements for the calculation of the turbulent flow around airfoils, wings and bodies of revolution. *AGARD CP* 271, *Paper* 16.

CEBECI, T. & SCHIMKE, S. M. 1983 The calculation of separation bubbles in interactive turbulent boundary layers. *J. Fluid Mech.* **131**, 305.

CEBECI, T. & SMITH, A. M. O. 1974 *Analysis of Turbulent Boundary Layers.* Academic.

CEBECI, T., STEWARTSON, K. & WILLIAMS, P. G. 1981 Separation and reattachment near the leading edge of a thin airfoil at incidence. *AGARD CP* 291, *Paper* 20.

CHANG, K. C., BUI, M. N., CEBECI, T. & WHITELAW, J. H. 1984 The calculation of turbulent wakes. *Mech. Engng Dept Rep.* ME-84-3. California State University, Long Beach.

COLES, D. & WADCOCK, A. J. 1979 Flying-hot-wire study of flow past an NACA 4412 airfoil at maximum lift. *AIAA J.* **17**, 321.

CRIMI, P. & REEVES, B. L. 1976 Analysis of leading-edge separation bubble on airfoils. *AIAA J.* **14**, 1548.

DAVIS, R. L. & CARTER, J. E. 1984 Analysis of airfoil transitional separation bubbles. *AIAA Paper* 84-1613.

GLEYZES, C., COUSTEIX, J. & BONNET, J. L. 1984 A calculation method of leading edge separation bubbles. In *Numerical and Physical Aspects of Aerodynamic Flows*, vol. II (ed. T. Cebeci), p. 173. Springer.

HALSEY, N. D. 1979 Potential flow analysis of multielement airfoils using conformal mapping. *AIAA J.* **17**, 1281.

HEAD, M. R. 1976 Eddy viscosity in turbulent boundary layers. *Aero. Quart.* **27**, 270.

KWON, O. K. & PLETCHER, R. H. 1979 Prediction of incompressible separated boundary layers including viscous–inviscid interaction. *Trans. ASME* I: *J. Fluids Engng* **101**, 466.

LEBALLEUR, J. C. 1978 Couplage visqueux–non-visquex : Méthode numérique et applications aux écoulements bidimensionnels transsoniques et supersoniques. *La Recherche Aérospatiale*, no. 1978-2, p. 65.

MCDONALD, H. & FISH, R. W. 1973 Practical calculation of transitional boundary layers. *Intl J. Heat Mass Transfer* **16**, 1729.

MCDONALD, H. & KRESKOVSKY, J. P. 1974 Effect of free stream turbulence on the turbulent boundary layer. *Intl J. Heat Mass Transfer* **17**, 705.

MCGHEE, R. J. & BEASLEY, W. D. 1973 Low-speed aerodynamic characteristics of a 17-percent thick airfoil section design for general aviation applications. *NASA TN* D-7428.

MCGHEE, R. J., BEASLEY, W. D. & SOMERS, D. M. 1977 Low-speed aerodynamic characteristics of a 13-percent thick airfoil section designed for general aviation applications. *NASA TMX* 72697.

MEHTA, U., CHANG, K. & CEBECI, T. 1986 A comparison of interactive boundary layer and thin-layer Navier–Stokes procedures. In *Numerical and Physical Aspects of Aerodynamic Flows*, vol. III (ed. T. Cebeci). Springer.

MELNIK, R. E. & BROOK, J. W. 1986 The computation of viscous/inviscid interaction on airfoils with separated flow. In *Numerical and Physical Aspects of Aerodynamic Flows*, vol. III (ed. T. Cebeci). Springer.

MICHEL, R. 1951 Etude de la transition sur les profiles d'aile; établissement d'un critère de détermination de point de transition et calcul de la trainée de profile incompressible. *ONERA Rep.* 1/1578A.

NAKAYAMA, A. 1982 Measurements in the boundary layer and wake of two airfoil models. *Douglas Aircraft Co. Rep. No.* MDC J2403. Long Beach, CA.

NARASIMHA, R. & PRABHU, A. 1972 Equilibrium and relaxation in turbulent wakes. *J. Fluid Mech.* **54**, 1.

NITUCH, M. J., SJOLANDER, S. & HEAD, M. R. 1978 An improved version of the Cebeci–Smith eddy-viscosity model. *Aero. Quart.* **29**, 207.

PATEL, V. C. & SCHEUERER, G. 1982 Calculation of two-dimensional near and far wake. *AIAA J.* **20**, 900.

RODI, W. 1975 A review of experimental data for uniform-density free turbulent boundary layers. In *Studies in Convection*, vol. 1 (ed. B. E. Launder). Academic.

SIMPSON, R. L., CHEW, Y. T. & SHIVAPRASAD, B. G. 1981 The structure of a separating turbulent boundary layer. Part I. Mean flow and Reynolds stresses. *J. Fluid Mech.* **113**, 23.

TOWNSEND, A. A. 1956 *The Structure of Turbulent Shear Flow*. Cambridge University Press.

VELDMAN, A. E. P. 1981 New quasi-simultaneous method to calculate interacting boundary layers. *AIAA J.* **19**, 769.

WADCOCK, A. J. 1978 Flying-hot-wire study of two-dimensional turbulent separation on an NACA 4412 airfoil at maximum lift. Ph.D. thesis, California Institute of Technology, Pasadena, CA.